High-pressure hydrides of iron and its alloys

2002 J. Phys.: Condens. Matter 14 6427

(http://iopscience.iop.org/0953-8984/14/25/311)

INSTITUTE OF PHYSICS PUBLISHING JOURNAL OF PHYSICS: CONDENSED MATTER

J. Phys.: Condens. Matter **14** (2002) 6427–6445 PII: S0953-8984(02)33717-2

High-pressure hydrides of iron and its alloys

V E Antonov[1], M Baier[2], B Dorner[3], V K Fedotov[1], G Grosse[2], A I Kolesnikov[1], E G Ponyatovsky[1], G Schneider[2] and F E Wagner[2]

[1] Institute of Solid State Physics RAS, 142432 Chernogolovka, Moscow District, Russia
[2] Physics Department, Technical University of Munich, 85747 Garching, Germany
[3] Institut Laue–Langevin, BP 156, 38042 Grenoble Cedex 9, France

Received 13 February 2002, in final form 21 May 2002
Published 14 June 2002
Online at stacks.iop.org/JPhysCM/14/6427

Abstract

Hydrides of iron and iron-based alloys are thermodynamically stable only at hydrogen pressures in the gigapascal range and rapidly lose hydrogen under ambient conditions. At low temperatures, however, these hydrides can be retained in a metastable state at atmospheric pressure after being cooled under high pressure to liquid nitrogen temperature. This review will discuss the current state of studies on phase transformations in the Fe–H and related systems and also on the composition, crystal structure and physical properties of the hydrides, both under high hydrogen pressures and in the 'quenched' metastable state at ambient pressure. The studies at ambient pressure include magnetization measurements, x-ray and neutron diffraction, Mössbauer spectroscopy and inelastic neutron scattering. In the sections on Mössbauer and structural investigations of hydrides of Fe–Cr and Ni–Fe alloys new experimental results will be presented.

1. Introduction

The iron–hydrogen and related systems have been extensively studied for many decades in connection with such technologically important problems as hydrogen-induced embrittlement and degradation of ferrous metals. More recently, hydrides of iron and iron-based alloys also gained a significant interest for geophysics and planetary science as candidates for the main constituents of the Earth's core [1–3]. Additionally, the possibility of studying these hydrides by ^{57}Fe Mössbauer spectroscopy makes them model objects for the investigation of local characteristics of hydrides, such as the hydrogen distribution near the iron atoms, the local magnetic fields or the electronic state of the iron atoms.

The equilibrium hydrogen solubility in iron at a H_2 pressure of 1 bar is very small and varies from a H-to-metal atomic ratio of $x \approx 10^{-6}$ at room temperature to $x \approx 10^{-3}$ near the melting temperature of iron [4]. Attempts to produce hydrides of iron by electrolysis have been unsuccessful, but iron hydride can be prepared by implantation of H^+ ions at liquid nitrogen temperature [5]. The preparation of bulk, homogeneous samples of iron hydrides

suitable for an accurate determination of their chemical composition, crystal structure and physical properties, however, is possible only under equilibrium conditions in an atmosphere of hydrogen at pressures of several gigapascals.

Iron hydride was synthesized for the first time at ISSP RAS in 1980 [6] using a technique for compressing gaseous hydrogen to pressures of up to 9 GPa at temperatures up to 500 °C [7] (later the temperature limit was extended to 1000 °C [8]). This technique allows *in situ* measurements of electrical resistance and magnetic permeability and also the rapid cooling of the hydrides under high pressure to liquid nitrogen temperature. At such a low temperature, hydrides of iron and its alloys are metastable at ambient pressure and can be removed from the high-pressure cell for investigation at ambient pressure. The amount of hydride produced in one experiment lies between 30 and 500 mm^3, which is enough for studies by many methods, including methods using neutron scattering.

Most results discussed in the present paper were obtained on samples prepared at ISSP RAS. Results significant for phase identification and for constructing the phase diagram of the Fe–H system were also obtained by a Japanese group from Chuo University, Tokyo [3, 9, 10], who developed a technique for *in situ* x-ray diffraction investigation of metal–hydrogen systems at pressures up to 7 GPa and temperatures up to about 2000 °C. The pressure of formation [11, 12] and decomposition [13] of iron hydride at room temperature and the pressure dependence of the lattice parameters of iron hydride at room temperature and pressures up to 62 GPa [11] were determined by three other research groups using diamond anvil cells and *in situ* x-ray diffraction [11, 13] or Mössbauer spectroscopy [12].

2. The Fe–H system

Iron belongs to the group VI–VIII transition metals, of which only Pd forms hydrides at low hydrogen pressures. The hydrides formed at high pressures in the systems other than Fe–H were shown to have close-packed metal sublattices with an fcc (γ) or hcp (ε) structure, in which hydrogen occupies octahedral interstitial positions (see [14, 15] for references). Most of these hydrides exist in wide composition ranges and can be considered as solid solutions of hydrogen distributed over the interstices either randomly or with a superstructure order. Hydrogen induces a rather large volume expansion $\Delta V_a(x)$ of the host metal that reaches 2–3 $Å^3$ per metal atom at $x = 1$ and can serve as an indicator of hydride formation.

Iron forms an ε' hydride with a *double hcp* metal lattice [16] and $x \approx 1$ [17], an fcc γ hydride of unknown composition [10] and also a metastable intermediate hcp ε phase [10] with $x \approx 0.4$ [18]. The ε'-FeH hydride is a ferromagnet with a spontaneous magnetization of $\sigma_0 \approx 2.2\ \mu_B$ per iron atom at $T = 0$ K and the Curie temperature much exceeding 300 K [19]. The ε-$FeH_{0.42}$ hydride is paramagnetic down to 4.2 K [18]. The magnetic properties of the γ hydride are not known yet. The hydrides rapidly decompose at ambient pressure on heating above 150 K.

The T–P diagram of phase transformations of iron placed in an atmosphere of gaseous hydrogen is shown in figure 1. It was constructed from the positions of anomalies of the pressure (figure 2(a)) and temperature (figure 2(b)) dependences of the electrical resistance and magnetic permeability determined with an accuracy of ± 0.3 GPa and ± 15 °C. The lines of phase transformations divide the T–P plane of the diagram into three regions: α, ε' and γ. The co-ordinates of the triple point are $T \approx 280$ °C and $P \approx 5$ GPa.

According to the phase rule, only single-phase fields are possible in the equilibrium T–P diagrams of binary Me–H systems, but the composition of every phase can vary continuously with T and P within the corresponding field. At temperatures up to 350 °C, the composition of the ε'-hydride is close to FeH independent of the pressure [11, 17, 18], while at higher

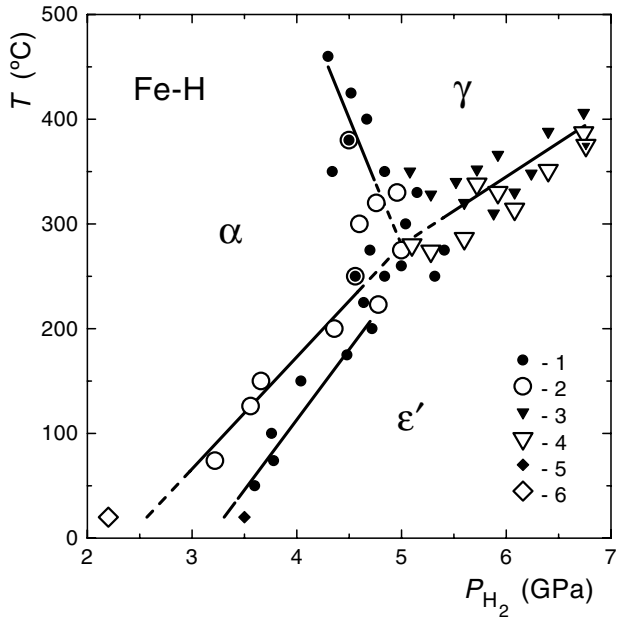

Figure 1. T–P phase diagram of the Fe–H system [20]. 1, 2 are the midpoints of anomalies of the electrical resistance isotherms measured at increasing and decreasing pressure, respectively (figure 2(a)); 3, 4 are the midpoints of anomalies of the isobars of electrical resistance and magnetic permeability measured at increasing and decreasing temperature, respectively (figure 2(b)); 5, 6 are the formation [11, 12] and decomposition [13] pressure of ε'-FeH at room temperature from measurements in diamond anvil cells. α is the dilute hydrogen solid solution in bcc α-Fe with $x < 0.01$ [20]; ε' is the approximately stoichiometric [17] ε'-FeH hydride with a *double* hcp metal lattice [16]; γ is the hydride with an fcc metal lattice [10] and as yet unknown composition.

temperatures a decrease in V_a indicates a gradual decrease of the hydrogen content [10]. The $\alpha \rightarrow \varepsilon'$ transition in the Fe–H system is very sluggish, and a noticeable amount of non-reacted α-Fe was observed even in Fe–H samples loaded with hydrogen at a pressure as high as 9 GPa at room temperature [11] and at 350 °C [16]. The considerable hysteresis of the $\alpha \leftrightarrow \varepsilon'$ transformation is caused by elastic stresses, which are close to the yield stress and appear to be due to the sudden increase in sample volume by about 16% upon hydride formation. The curve of thermodynamic equilibrium between the α- and ε'-phase therefore should be close to the $\varepsilon' \rightarrow \alpha$ curve of hydride decomposition, since removal of hydrogen leads to the relaxation of accumulated elastic stresses. This is characteristic of phase transformations in all metal–hydrogen systems at high pressures [21], and the $\varepsilon' \rightarrow \alpha$ curve in figure 1 is likely to well represent the phase equilibrium.

In situ x-ray studies at a hydrogen pressure of 6 GPa and elevated temperatures showed [10] that the γ-phase has an fcc metal lattice and nearly the same volume V_a per metal atom as the ε' hydride under the same conditions, so the γ-phase was assumed to be an iron hydride as well. Further x-ray investigations allowed the Japanese group to outline the T–P diagram of the Fe–H system over a wide range of temperatures and pressures [9] (figure 3(b)). Its comparison with the T–P diagram of Fe in inert media (figure 3(a)) shows that the γ-phase can be considered as a solid solution of hydrogen in the allotropic γ modification of Fe. However, all efforts to quench the γ-phase under pressure for further studies at ambient pressure were unsuccessful [20], and its composition and physical properties still remain unknown.

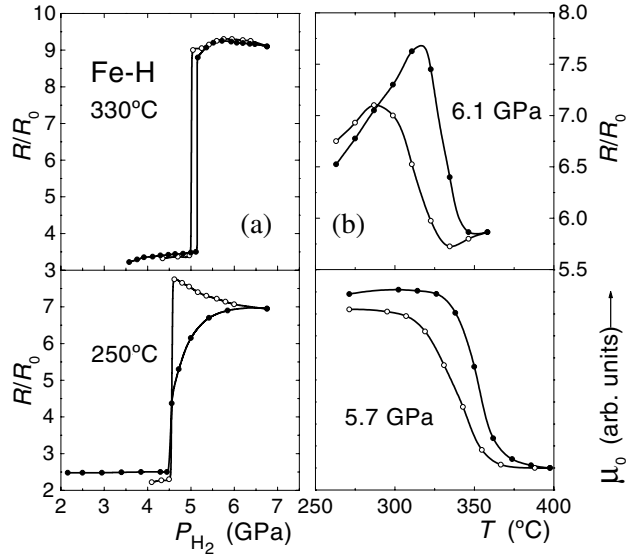

Figure 2. Representative isotherms of the electrical resistance (a) and isobars of the electrical resistance and magnetic permeability (b) of iron measured at increasing (solid circles) and decreasing (open circles) pressure or temperature in a hydrogen atmosphere [20]. R_0 is the initial resistance of the sample at ambient temperature and pressure.

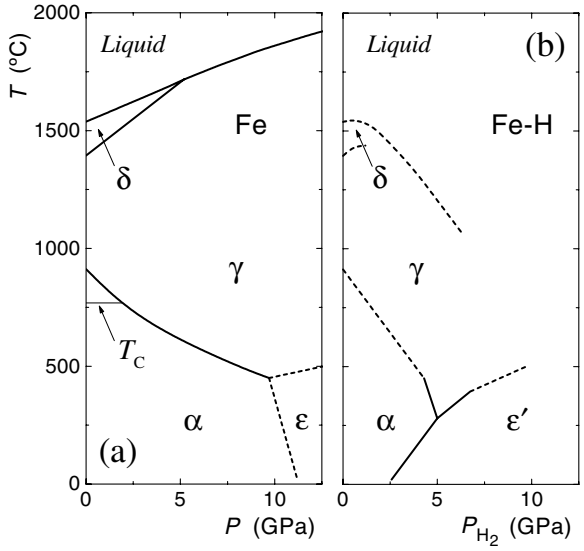

Figure 3. T–P phase diagrams of Fe in inert media [22] (a) and in a hydrogen atmosphere (b). The solid lines in (b) represent the phase boundaries from [20] shown in figure 1; the dashed lines show tentative boundaries in the extended T–P region according to the *in situ* x-ray diffraction studies of [9]. The letters in (a) and (b) mark the fields of phases with different metal lattices: α, δ = bcc, γ = fcc, ε = hcp, ε' = dhcp. T_C is the Curie temperature of ferromagnetic α-Fe.

X-ray diffraction [10] also showed that the $\alpha \rightarrow \varepsilon'$ transition at elevated temperatures is a complex process involving formation of an intermediate ε-phase with an hcp metal lattice and a volume per metal atom, V_a, lying somewhere in between those for pure hcp ε-Fe and

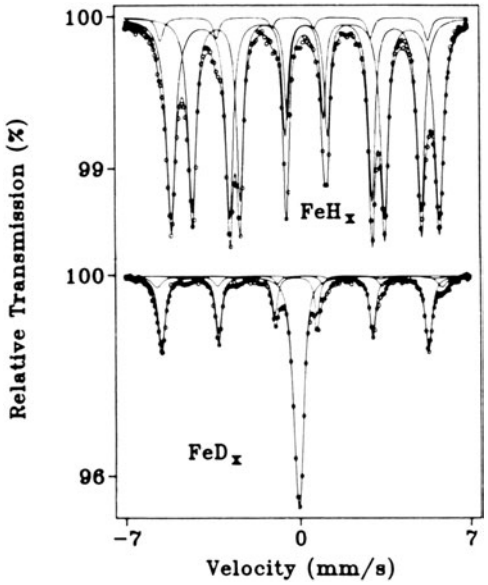

Figure 4. Representative ^{57}Fe Mössbauer spectra of Fe–H and Fe–D samples measured at 4.2 K with a ^{57}Co:Rh source also at 4.2 K [17]. The spectrum of the Fe–H sample consists of two magnetic patterns of ε'-FeH with nearly equal intensities (53 and 43%) and a weak (4%) sextet of α-Fe. The main components of the Fe–D spectrum are the non-magnetic single-line pattern of the ε-phase (41%) and the magnetic sextet of α-Fe (44%).

Table 1. The main components of the ^{57}Fe Mössbauer spectra shown in figure 4. S is the isomer shift with respect to the source of ^{57}Co in rhodium at 4.2 K; ΔE_Q the effective electric quadrupole interaction; B_{hf} is the magnetic hyperfine field; RI is the relative intensity of the individual components.

Sample	S (mm s^{-1})	ΔE_Q (mm s^{-1})	B_{hf} (T)	RI (%)	Assignment
Fe–H	+0.364(5)	−0.053(5)	33.8(1)	53(1)	ε'-FeH, site 'h'
	+0.370(5)	+0.030(5)	28.8(1)	43(1)	ε'-FeH, site 'c'
	−0.122(5)	0.0	33.8(1)	4(1)	α-Fe
Fe–D	−0.037(5)	—	—	41(2)	ε-FeH$_x$, $x \sim 0.3$
	−0.128(5)	0.0	33.7(1)	44(1)	α-Fe

ε'-FeH. Similar to ε'-FeH, the ε-phase can be quenched at high pressure and studied at ambient pressure. Studies performed on such quenched ε'- and ε-phase samples will now be discussed.

Figure 4 and table 1 present the results of a Mössbauer investigation of the Fe–H and Fe–D samples synthesized at 350 °C and H_2 or D_2 pressures of about 9 GPa [17]. The Fe–H sample was nearly pure ε'-hydride, while the Fe–D sample contained the maximum amount of the ε-phase obtained in that work. (No evident relationship has been found so far between the amount of the ε-phase in the sample and the conditions of synthesis within the ε' field of the T–P diagram; the content of the ε-phase was, however, usually larger in samples loaded with deuterium than in samples loaded with hydrogen.)

In the dhcp iron lattice of ε'-FeH, there are two crystallographically inequivalent iron sites, i.e. 'hexagonal' and 'cubic' ones, arranged in close-packed layers that lie, respectively, between adjacent layers stacked in the same way or stacked differently. Accordingly, as was first observed in [23], the ^{57}Fe Mössbauer spectrum of ferromagnetic ε'-FeH consists of two

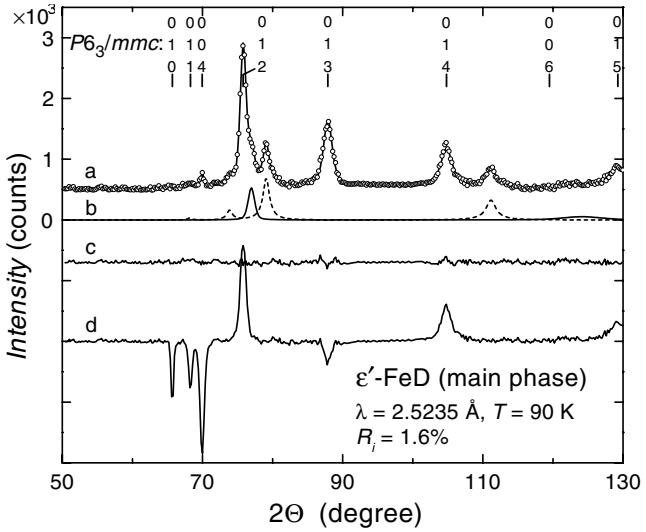

Figure 5. Neutron diffraction pattern of an Fe–D sample (circles) and results of its Rietveld analysis (lines) involving ε'-FeD (the main phase) and ε-$FeD_{0.42}$ and α-Fe [18]. The final values of the fit parameters are listed in table 2. (a) Calculated profile shown as a solid curve; (b) calculated contributions from ε-$FeD_{0.42}$ (dashed curve) and from α-Fe (solid curve); (c) difference between the experimental (circles) and calculated (curve (a)) spectra; (d) difference between the experimental spectrum and that calculated for deuterium randomly occupying half of the tetrahedral interstitial sites in the dhcp lattice of ε'-FeD, the other fit parameters being the same as in table 2. The indices in the upper part of the figure refer to ε'-FeD.

magnetic six-line patterns, which have practically the same isomer shift (figure 1 and table 1). The pattern with the larger hyperfine field B_{hf} has a negative effective electric quadrupole interaction ΔE_Q, while the pattern with the smaller B_{hf} has a positive ΔE_Q. The pattern with the negative ΔE_Q was ascribed to Fe atoms on the 'hexagonal' sites [17], because the electric quadrupole interaction is negative for Fe substituting Co in ferromagnetic cobalt hydrides with an hcp metal lattice composed of equally stacked 'hexagonal' close-packed layers (the Co hydrides were studied in the same work [17]). The Mössbauer spectra of hydrides of Fe–Cr alloys discussed later in the present work lend further credence to this attribution. The ideal dhcp stacking sequence is . . . hchchc . . . with equal numbers of 'h' and 'c' layers. Interestingly, the area under the 'h' pattern is about 20% larger than that under the 'c' pattern (table 1). The difference was attributed to the presence of stacking faults in the dhcp iron lattice of ε'-FeH leading to the increase in the number of 'h' layers.

The single-line pattern from the ε-phase in the Fe–D sample shown in figure 4 suggests that this phase is not magnetically ordered at 4.2 K. The isomer shift of the pattern corresponds to the hydrogen content of the ε-phase of $x \approx 0.3$ [17].

One Fe–H sample consisting nearly entirely of ε' hydride and two Fe–D samples containing the minimum and the maximum amounts of the ε-phase were studied by neutron diffraction [18]. The samples contained a few per cent of non-reacted α-Fe. The structures of all phases were refined using Rietveld profile analysis. The diffraction pattern of one sample and the results of its profile fit are illustrated by figure 5. The proposed crystal structures of the ε'- and ε-phases are schematically shown in figure 6. The refined parameters of these phases are listed in table 2.

The profile fit showed that the composition of the ε-phase is ε-$FeD_{0.42(4)}$ and that deuterium randomly occupies octahedral interstices in its hcp metal lattice (open circles in figure 6). The

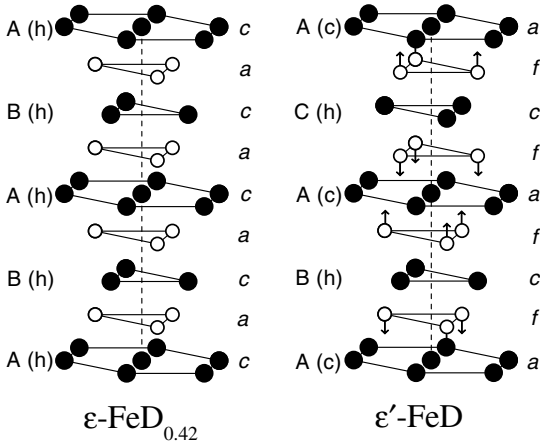

Figure 6. Crystal structures of ε'-FeD and of ε-$FeD_{0.42}$ [18]. The letters a, c and f mark layers of equivalent positions in the $P6_3/mmc$ space group originating, respectively, from positions 2a, 2c and 4f with $Z = 0.882 \approx 7/8$ (table 2). The solid circles show regular positions of Fe atoms, open circles of D atoms. The arrows indicate the directions of the displacements of D atoms from the centres of the octahedral interstices in ε'-FeD. The letters A, B and C represent the standard notation for close-packed layers in the hcp and dhcp structures; (h) and (c) indicate layers of 'hexagonal' and 'cubic' metal sites.

Table 2. Positional parameters (X, Y, Z) and site occupancies for iron hydride and deuterides according to the Rietveld profile analysis of the neutron diffraction data collected at 90 K using the D1B diffractometer at ILL, Grenoble. M is the number of formula units per unit cell; N is the number of atoms per unit cell.

Phase	Atom	Site	X	Y	Z	Occupancy	N
ε'-FeH, $P6_3/mmc$, $M = 4$	Fe	2a	0	0	0	1.000	2.00
$a = 2.679$ Å, $c = 8.77$ Å,	Fe	2c	1/3	2/3	1/4	0.935	1.87
$c/a = 2 \times 1.637$	H	4f	1/3	2/3	7/8	0.935	3.74
	Fe	2d	1/3	2/3	3/4	0.065	0.13
	H	4f	1/3	2/3	1/8	0.065	0.26
ε'-FeD, $P6_3/mmc$, $M = 4$	Fe	2a	0	0	0	1.000	2.00
$a = 2.668$ Å, $c = 8.75$ Å,	Fe	2c	1/3	2/3	1/4	0.845	1.69
$c/a = 2 \times 1.640$	D	4f	1/3	2/3	0.882	0.845	3.38
	Fe	2d	1/3	2/3	3/4	0.155	0.31
	D	4f	1/3	2/3	0.118	0.155	0.62
ε-$FeD_{0.42(4)}$; $P6_3/mmc$, $M = 2$	Fe	2c	1/3	2/3	1/4	1.00	2.00
$a = 2.583$ Å, $c = 4.176$ Å,	D	2a	0	0	0	0.42	0.84
$c/a = 1.617$							

octahedral hydrogen coordination is characteristic of all hcp and fcc hydrides of the group VI–VIII transition metals studied so far. Unlike ε-$FeD_{0.42(4)}$, however, the two other known ε hydrides with $x \approx 1/2$, $CoD_{0.5}$ [15] and $TcH_{0.45}$ [24], form layered superstructures of the anti-CdI_2 type with D or H atoms preferentially occupying every second basal layer of octahedrons.

In the ε'-phase, hydrogen or deuterium also fill octahedral interstitial positions, the alternative tetrahedral model being completely inadequate, as is shown by the difference

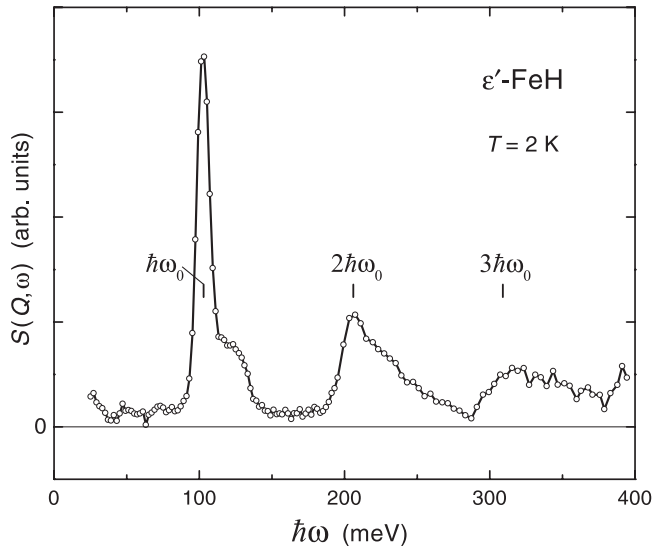

Figure 7. The dynamical structure factor $S(Q, \omega)$ of ε'-FeH as a function of the energy loss $\hbar\omega$ of the inelastically scattered neutrons measured at 2 K [25]. The main optical hydrogen peak is at $\hbar\omega_0 = 103$ meV.

curve (d) in figure 5. The excessive number of iron 'h' layers due to stacking faults [17] resulted in a significant decrease of the intensities of those diffraction lines of the dhcp structure that are 'superstructural' for the corresponding hcp lattice (in figure 5 these are the (013) and (015) lines). To incorporate stacking faults into the calculation scheme for the space group $P6_3/mmc$, partial occupation of 'defect' d sites by Fe atoms and f sites with $Z \approx 1/8$ by H or D atoms was allowed along with occupation of 'regular' sites. As seen from table 2, the obtained number N of H or D atoms on 'defect' sites is twice as large as that of Fe for both ε'-FeH and ε'-FeD. This can be regarded as a successful self-test of the model, since a replacement of a c layer of iron atoms by a d layer, which is just a rotation of the layer through an angle of 60°, will also rotate two adjacent hydrogen (deuterium) layers from regular to defect f positions.

The neutron scattering amplitudes of D and H atoms are significantly different, and, in contrast to the neutron diffraction pattern of ε'-FeH, the pattern of ε'-FeD exhibits intensive peaks at large angles. This allowed a more accurate analysis of possible displacements of D atoms from the centres of octahedral interstices along the c-axis. The optimization procedure yielded $\delta Z = 0.007 \times c \approx 0.06$ Å (table 2). Though the effect was largely within the error limits, such displacements are very likely on physical grounds, as they increase the distance between deuterium atoms in equally stacked octahedral layers, which is the shortest distance between any deuterium atoms in the ε'-FeD structure. A tendency to increase the D–D distance is expected in view of the strong long-range repulsive interaction between hydrogen atoms, which is one of the main factors governing the formation of transition-metal hydrides [14].

The spectrum of optical hydrogen vibrations in ε'-FeH has been studied by inelastic neutron scattering (INS) using the IN1 BeF spectrometer at ILL, Grenoble [25]. The spectrum is shown in figure 7 and looks similar to the INS spectra of hydrides of all other 3d and 4d metals of groups VI–VIII studied so far. The first, fundamental band of optical H vibrations consists of a strong peak centred at $\hbar\omega_0 = 103$ meV with a broad shoulder towards higher energies. Based on results for palladium hydride [26], the main peak is usually ascribed to nearly non-dispersive transverse optical modes, while the shoulder is assumed to arise from longitudinal

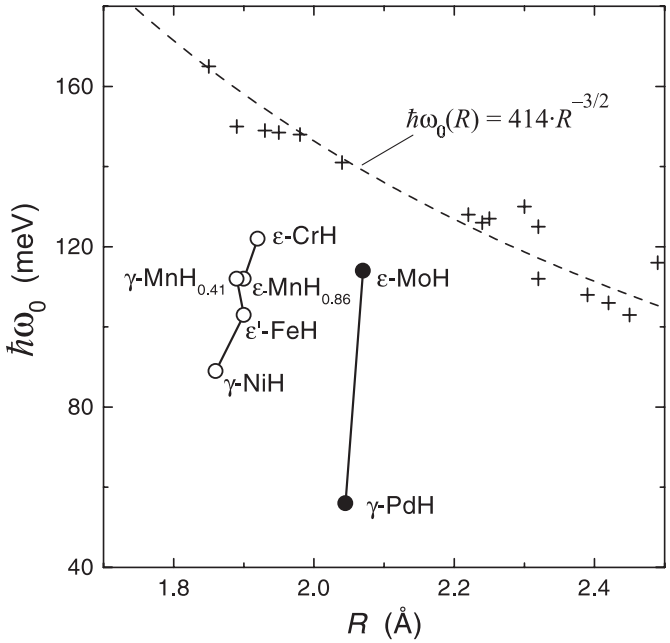

Figure 8. Energy of the main optical hydrogen peak, $\hbar\omega_0$, versus the shortest hydrogen–metal distance R for various dihydrides with a fluorite-type structure (crosses) [27] and for monohydrides of 3d metals (open circles) and 4d metals (solid circles) (see [28] for references). The dashed curve is a least-squares fit to the data for the dihydrides.

optical modes, which show significant dispersion due to long-range repulsive H–H interactions. The second and the third optical H band have a smoother intensity distribution and appear at energies approximately two and three times the energy of the fundamental band, respectively. As a function of the hydrogen–metal distance R, the value of $\hbar\omega_0$ for ε'-FeH agrees well with the approximately linear dependence $\hbar\omega_0(R)$ for ε and γ hydrides of 3d metals (figure 8).

3. Hydrides of iron alloys

3.1. The rigid-d-band model

Concentration dependences of the spontaneous magnetization σ_0 at $T = 0$ K (for ferromagnets) and of the Néel temperature T_N (for antiferromagnets) of fcc (γ) alloys of 3d metals which are close neighbours in the periodic table are well described by the rigid-band model and can be represented as unique functions of the average number N^e of external (3d + 4s) electrons per atom of the alloy (the so-called Slater–Pauling curves). These dependences are plotted by thin solid curves in figure 9. Our studies of γ hydrides of fcc Ni-based and Fe-based alloys showed [7, 29] that the magnetic properties changed with increasing hydrogen content as if the hydrogen were merely a donor of a fractional number of $\eta \approx 0.5$ electrons per H atom in the otherwise unchanged metal d band. This approximation, which we call the rigid-d-band model for brevity, is a rather straightforward consequence of the available *ab initio* band structure calculations, and its applicability to alloys with different types of band structure has been thoroughly discussed in [7]. In particular, if the properties of the alloy obey the rigid-band model, the properties of its γ hydrides considered as functions of the effective electron concentration $N^e(x) = N^e(0) + \eta x$ are described by the thin curves of figure 9.

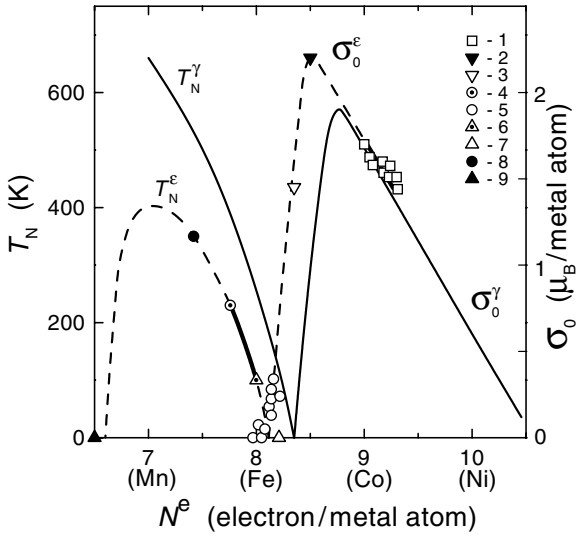

Figure 9. Slater–Pauling curves for fcc (γ) alloys (experiment—thin solid curves) and hcp (ε) alloys (experiment—two sections of thick solid curves; an estimation—dashed curves) of 3d metals that are nearest neighbours in the periodic table. The symbols show experimental data for hydrides presented as a function of the effective electron concentration, $N^e(x) = N^e(0) + \eta x$, with $\eta = 0.5$ electrons per H atom: 1—σ_0 of ε-CoH_x solid solutions [30]; 2–σ_0 of ε'-FeH [19]; 3–σ_0 of $Fe_{0.947}Cr_{0.053}H_{0.92}$ with a $9R$-type metal lattice [16]; 4— T_N of ε-Fe [31]; 5—σ_0 of ε-$FeH_{0.42}$ [18]; 6–T_N of ε-$Fe_{0.776}Mn_{0.224}$ [32]; 7—σ_0 of ε-$Fe_{0.776}Mn_{0.224}H_x$ solid solutions [33]; 8— T_N of ε-$Mn_{0.83}$ [34]; 9—T_N of ε-CrH [35].

Due to the relatively narrow intervals of mutual solubility of 3d metals in hexagonal phases, the concentration dependences of their magnetic properties are known to a much lesser extent than those of the fcc alloys (two segments of thick solid line in figure 9). However, if the available experimental points for hexagonal hydrides are added to the graph as a function of $N^e(x)$ with $\eta = 0.5$ electrons per H atom, the properties of both hexagonal metals and hydrides can be described by the same curves (dashed curves in figure 9). These curves are similar to those for the γ alloys and are likely to represent the Slater–Pauling plot for the (hypothetical) hexagonal alloys.

3.2. Hydrides of Fe–Cr alloys

Three bcc (α) Fe–Cr alloys containing 50, 25 and 5.3 at.% Cr were loaded with hydrogen at 325 °C and various H_2 pressures up to 7 GPa, and the resulting hydrides were studied in a metastable state at ambient pressure by x-ray diffraction and magnetization measurements [16]. The hydrides of alloys containing 25 and 50 at.% Cr were found to have an hcp metal lattice like CrH [14]. At a Cr content of 5.3 at.%, the hexagonal close packed structure has been found to contain stacking faults ordering at least partially into a $9R$ structure, which may be considered as a transitional state between the hcp metal lattice of the Cr-rich alloys and the dhcp structure of the hydride of pure iron. The hydrides of Fe–Cr alloys with hydrogen-to-metal ratios close to unity have been found to be ferromagnetic or at least contain ferromagnetic fractions up to Cr contents of 25 at.%.

In the present work, ^{57}Fe Mössbauer experiments were performed at 4.2 K on hydrides of the same three Fe–Cr alloys, which were loaded with hydrogen at 325 °C and pressures

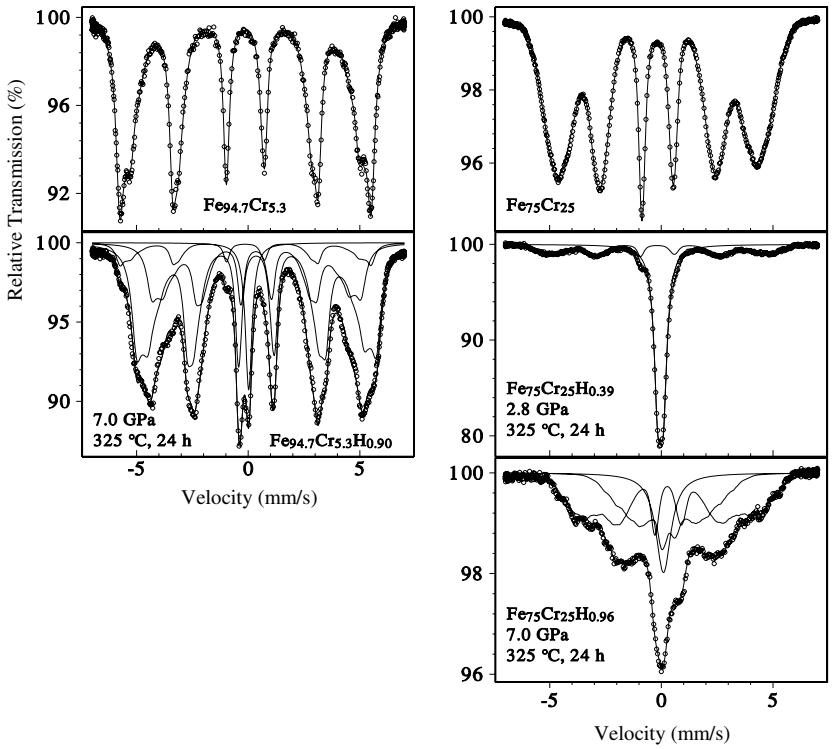

Figure 10. Mössbauer spectra of Fe–Cr alloys and their hydrides measured at 4.2 K with a ^{57}Co:Rh source also at 4.2 K.

of 2.8 and 7 GPa. The results of the Mössbauer experiments are largely in agreement with the magnetic properties of the hydrides of Fe–Cr alloys, but they yield additional information on the individual lattice sites and phases.

The Mössbauer pattern of α-$Fe_{0.947}Cr_{0.053}$ (figure 10) resembles those reported by Dubiel and Inden [36] for Fe–Cr alloys of similar composition and was fitted by the model suggested by these authors, which assumes that m nearest and n next-nearest Cr neighbours reduce the hyperfine field at the Fe by $m\Delta H_1$ and $n\Delta H_2$, respectively, and that the distribution of Cr atoms around the iron is binomial. The spectrum of $Fet_{0.947}Cr_{0.053}H_{0.90}$ (figure 10) can largely be described as a superposition of two such patterns, one for the 'h' sites and one for the 'c' sites in the, at least approximate, $9R$ structure of the hydride. With 33.3 and 29.1 T, the fields for iron in $Fe_{0.947}Cr_{0.053}H_{0.90}$ with $m = n = 0$ are nearly the same as those for the two sites in the dhcp iron hydride [17]. In $Fe_{0.947}Cr_{0.053}H_{0.90}$, however, the component with the bigger hyperfine field is about twice as strong as that with the smaller field.

In the $9R$ structure, there are twice as many 'h' sites as 'c' sites. The Mössbauer pattern with the higher field must thus be attributed to the 'h' sites, and that with the lower field to the 'c' sites. This confirms the previous attribution of the Mössbauer component with the higher field in dhcp iron hydride to the 'h' sites [17].

The isomer shift of both Mössbauer components in $Fe_{0.947}Cr_{0.053}H_{0.90}$ with respect to α-$Fe_{0.947}Cr_{0.053}$ is 0.49 mm s^{-1}, which is practically the same as the shift between ε'-FeH and α-Fe.

The spectrum of $Fe_{0.947}Cr_{0.053}H_{0.90}$ also contains a minor magnetically split contribution of α-$Fe_{0.947}Cr_{0.053}$ and a weak single line with a width of 0.48 mm s^{-1} and a shift of 0.14 mm s^{-1}

with respect to α-$Fe_{0.947}Cr_{0.053}$. The presence of the non-magnetic component in the spectrum of $Fe_{0.947}Cr_{0.053}H_{0.90}$ is reminiscent of the single line observed in some hydrides and deuterides of pure iron [17], which has a similar isomer shift with respect to α-Fe (table 1). This isomer shift indicates that the hydrogen content of the non-magnetic phase is smaller than that of the magnetic hydride. The absence of ferromagnetism at low hydrogen contents is in agreement with the rigid-d-band model, according to which hexagonal or cubic close-packed Fe ($N^e = 8$ electrons per atom) and Fe–Cr alloys ($N^e < 8$ electrons per atom) must contain a certain amount of hydrogen to become ferromagnetic, as one can see from figure 9.

$Fe_{0.75}Cr_{0.25}H_{0.39}$ (figure 10) yields mainly a single line with an isomer shift of 0.08 mm s^{-1} with respect to hydrogen-free α-$Fe_{0.947}Cr_{0.053}$. The weak magnetically split fraction in this spectrum represents a minor residue of the hydrogen-free $Fe_{0.75}Cr_{0.25}$ alloy according to its isomer shift and hyperfine field. Assuming that this fraction of the sample contains no hydrogen at all, one concludes that the hydride giving rise to the unsplit Mössbauer line has a hydrogen-to-metal ratio near $x = 0.6$, for which the hydrides are, indeed, expected to be non-magnetic according to the rigid-d-band model, because this composition corresponds to only $N^e(0.6) \approx 7.8$ electrons per metal atom. According to the rigid-d-band model, the hydrides should, however, become ferromagnetic at higher x. This is borne out by $Fe_{0.75}Cr_{0.25}H_{0.96}$, which gives rise to a broad, unresolved magnetic Mössbauer pattern (figure 10), with a weak (12%) single-line contribution. This non-magnetic phase may be due to inhomogeneities in the hydrogen distribution.

$Fe_{0.50}Cr_{0.50}H_x$ hydrides with $x = 0.81$ and 0.99 are non-magnetic and give rise to somewhat broadened single Mössbauer lines with isomer shifts of 0.23 and 0.35 mm s^{-1} with respect to hydrogen-free α-$Fe_{0.947}Cr_{0.053}$. It is again in agreement with the rigid-d-band model that at a Cr content of 50% the hcp hydrides should no longer become ferromagnetic even at $x = 1$.

3.3. Solid solutions of hydrogen and deuterium in the fcc $Ni_{0.8}Fe_{0.2}$ alloy

Nickel hydride is formed via an isomorphous $\gamma_1 \rightarrow \gamma_2$ transition that terminates in a critical point of the liquid–vapour type at $T_{cr} \approx 390\,^{\circ}C$ and a hydrogen pressure of $P_{cr} \approx 1.75$ GPa [37]. Iron and nickel form an fcc disordered substitutional solid solution within a wide concentration range. Alloying of fcc Ni with Fe decreases T_{cr}, and the solubility of hydrogen in the Ni–Fe alloys containing more than about 15 at.% Fe is a continuous function of pressure at $T > 20\,^{\circ}C$ [38, 39].

Hydrogen is known to form continuous γ-solutions at room temperature with many Ni-based and Pd-based alloys. X-ray diffraction studies showed that a characteristic feature of most such solutions, including Ni–Fe–H, is a significant decrease in the slope of the $\Delta V_a(x)$ dependence at H-to-metal atomic ratios $x \geqslant 0.7$–0.8 (see [9] for a compilation of experimental results and references). The effect has already been debated for some decades and various explanations have been proposed, such as filling of the d band [40], formation of vacancies in the metal sublattice [7] and even metallization of the hydrogen sublattice [41]. However, none of the explanations has had adequate experimental grounds so far.

To learn more about the origin of the non-linear $\Delta V_a(x)$ dependence and about the hydrogen distribution over interstitial sites in the metal lattice, we carried out an x-ray, neutron diffraction and ^{57}Fe Mössbauer investigation of solid solutions of hydrogen and deuterium in the fcc Ni–Fe alloy containing 20 at.% Fe.

3.3.1. X-ray and neutron diffraction studies. Foils of a disordered substitutional $Ni_{0.8}Fe_{0.2}$ alloy were loaded with hydrogen or deuterium by a 24 h exposure to a H_2 or D_2 atmosphere

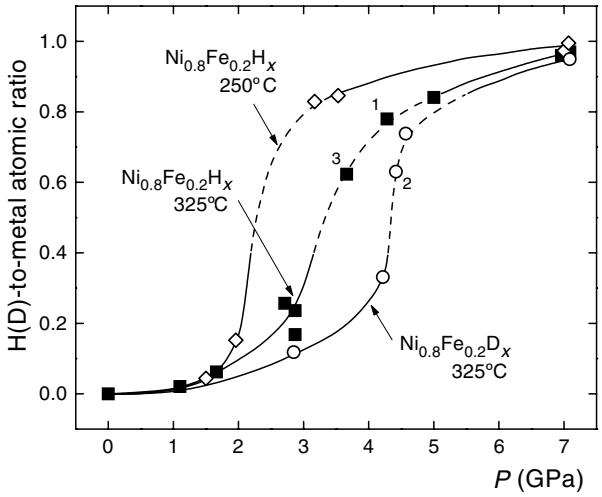

Figure 11. Isothermal absorption relationships between H_2 or D_2 gas pressure and H or D content x, respectively, of a $Ni_{0.8}Fe_{0.2}$ alloy. Numbers 1, 2 and 3 mark the points for the same samples in figures 11 and 12. Sample 3 was prepared differently from the others (see the text).

at a given pressure and at temperatures of 325 or 250 °C, followed by cooling to 150 K under pressure in order to avoid H or D losses from the samples when the pressure was released. The synthesis pressure was measured with an accuracy of ±0.3 GPa, the temperature with an accuracy of ±7 °C. The mean hydrogen or deuterium content of the obtained samples was determined with an accuracy of 2% by hot extraction at temperatures up to 500 °C. The resulting pressure–composition isotherms are shown in figure 11.

The x-ray diffraction studies showed that all the $Ni_{0.8}Fe_{0.2}H_x$ and $Ni_{0.8}Fe_{0.2}D_x$ foils were single phase and had an fcc metal lattice. The obtained values of $\Delta V_a(x)$ are shown by open symbols in figure 12. Similar to analogous dependences found in the literature [9], the $\Delta V_a(x)$ dependence thus obtained can be approximated with two straight lines, one below and one above $x = 0.7$. These lines are shown dashed in figure 12 and their slopes, $\beta = (\partial/\partial x)\Delta V_a(x) = 2.67$ and 0.93 Å^3 per metal atom per H(D) atom, are close to those for other γ-solutions of hydrogen in nickel and palladium alloys [9].

Some of the $Ni_{0.8}Fe_{0.2}H_x$ and $Ni_{0.8}Fe_{0.2}D_x$ samples were also studied by neutron diffraction at 124 K with the D20 diffractometer at ILL, Grenoble. To avoid texture effects, the samples had been previously powdered in an agate mortar under liquid nitrogen. Typical results are shown in figure 13. The $Ni_{0.8}Fe_{0.2}H_x$ solid solutions are ferromagnets and their spontaneous magnetization at 124 K decreases approximately linearly from 1.1 μ_B per metal atom at $x = 0$ to 0.6 μ_B per metal atom at $x = 1$ [39]. To reduce the number of fitting parameters, the magnetic contribution to the scattering intensity (curves (b) in figure 13) was calculated using the values of spontaneous magnetization given by this experimental linear dependence. A model assuming H or D atoms randomly distributed over the centres of octahedral interstitial positions in the fcc metal lattice gave a good profile fit of each diffraction pattern, while an occupation of tetrahedral interstices by hydrogen was found to be inconsistent with the experiments.

The values of $\Delta V_a(x)$ with both ΔV_a and x determined from the profile fit of the neutron diffraction data are shown in figure 12 by solid symbols. Two samples, with $x \approx 0.8$ and 0.63 (the corresponding points in figure 12 are labelled 1 and 2), showed a significant decrease in the lattice parameters after powdering. X-ray studies of the powdered samples gave the same new values of the lattice parameters as neutron diffraction.

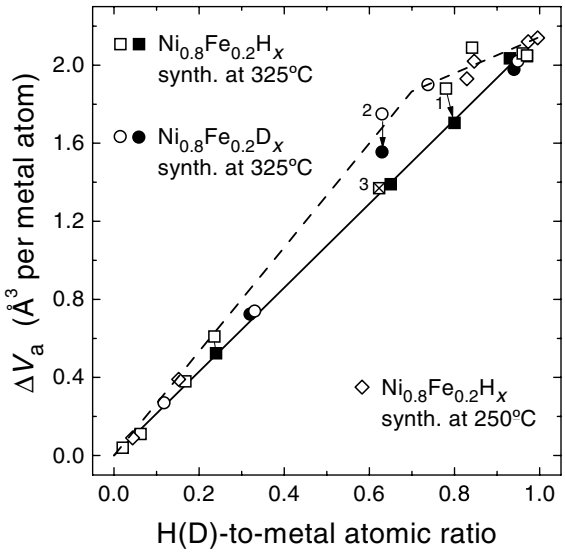

Figure 12. The dependence of $\Delta V_a = [a^3(x)–a^3(0)]/4$ on x for fcc $Ni_{0.8}Fe_{0.2}H_x$ and $Ni_{0.8}Fe_{0.2}D_x$ solid solutions. The open symbols show the results of x-ray diffraction studies on foils at 100 K; the hydrogen or deuterium contents were obtained by hot extraction. The solid symbols refer to neutron diffraction measurements on powdered samples at 124 K, the H or D contents resulting from the structure refinement. The arrows connect the points for the same samples before and after the powdering. $a(0) = 3.539$ Å.

As no hydrogen losses should occur in the course of the powdering under liquid nitrogen, the observed decrease in the lattice parameters suggests that the samples with $x \approx 0.8$ and 0.63 were inhomogeneous. In fact, with Fe Kα radiation used, the x-ray diffraction patterns from the 250 μm thick foils were formed only by surface layers with a thickness of a few micrometres. Therefore, about 98% of the sample volume remained unexplored. In contrast, the neutron measurements gave diffraction patterns averaged over the entire sample volume. The x-ray diffraction on the powdered samples would also give effectively volume-averaged patterns. The results of the diffraction studies of the samples with $x \approx 0.8$ and 0.63 before and after powdering can be understood if the surface layers of the foils of these samples are assumed to have had a higher hydrogen concentration and a larger lattice parameter than the inner parts.

The neutron diffraction pattern of the $Ni_{0.8}Fe_{0.2}H_{0.8}$ sample showed no traces of the hydrogen-rich surface phase. The lines of the main phase were narrow and the profile fit converged to a good ratio $R_p/R_{ex} = 1.7/1.9$ of the obtained and expected profile factors, indicating a good homogeneity of the specimen. Since a 5% admixture of a hydrogen-rich phase would be clearly seen in the diffraction pattern, we can roughly estimate that such a phase could form a layer no thicker than 15 μm on the surface of the 250 μm thick disc, while the remaining >95% disc volume consisted of a homogeneous phase with a lower hydrogen concentration. Thus, the hydrogenation of the sample with $x \approx 0.8$ must have been controlled by processes in a thin surface layer, while the diffusion rate in the bulk was high enough to provide a uniform hydrogen distribution.

The $Ni_{0.8}Fe_{0.2}D_{0.63}$ sample appeared inhomogeneous throughout. The irregular profile of its broadened neutron diffraction lines could not be fitted accurately at high diffraction

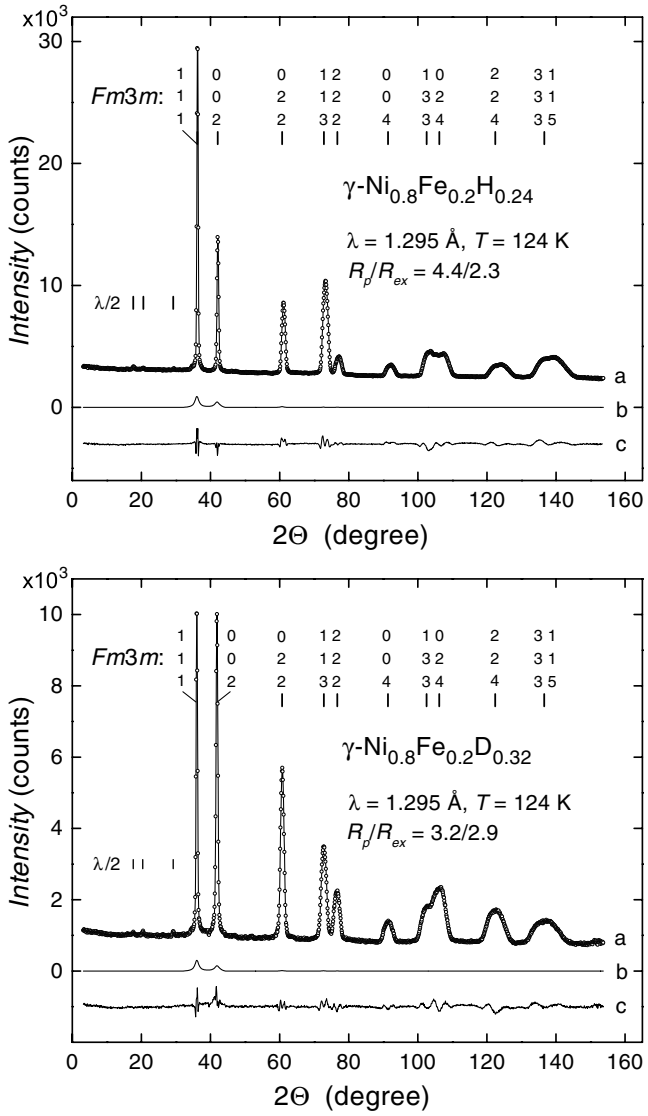

Figure 13. Neutron diffraction patterns of the $Ni_{0.8}Fe_{0.2}H_{0.24}$ and $Ni_{0.8}Fe_{0.2}D_{0.32}$ powder samples measured at 124 K (circles) and results of their Rietveld analysis (solid curves). Curve a is the profile calculated for hydrogen/deuterium on octahedral interstices and with the magnetic contribution shown by curve b. Curve c is the difference between the experimental (circles) and calculated (curve a) spectra.

angles, which resulted in $R_p/R_{ex} = 9.3/4.5$ and a large uncertainty in the x value. The observed inhomogeneity suggests a low rate of hydrogen diffusion in the bulk of the sample with $x \approx 0.63$.

As seen from figure 11, the $Ni_{0.8}Fe_{0.2}H_{0.8}$ and $Ni_{0.8}Fe_{0.2}D_{0.63}$ samples were synthesized in the ranges of a steep increase in the $x(P)$ isotherms. These are the ranges of supercritical anomalies of the isomorphous $\gamma_1 \leftrightarrow \gamma_2$ transformation terminating in a critical point at a lower temperature. A characteristic feature of such T–P ranges is a strong decrease in the H or D

diffusion rate. In our case, the centres of the supercritical regions correspond to $x \approx 0.5$. This explains the large inhomogeneity of the $Ni_{0.8}Fe_{0.2}D_{0.63}$ sample with the composition close to this critical value, the better homogeneity of the $Ni_{0.8}Fe_{0.2}H_{0.8}$ sample and a rather uniform distribution of H or D across the width of the samples with $x < 0.3$ and $x > 0.9$, which follows from the coincidence of the x-ray and neutron diffraction data for these samples (figure 12).

To demonstrate that the inhomogeneous state of the samples with intermediate values of x was due to the low rate of H or D diffusion, one sample, $Ni_{0.8}Fe_{0.2}H_{0.64}$, labelled 3 in figures 11 and 12, was prepared differently from others. Prior to the 24 h hydrogenation at 3.66 GPa and 325 °C, this sample was exposed to the same hydrogen pressure at 380 °C for 8 h in order to accelerate the hydrogen diffusion and to achieve a more uniform initial hydrogen distribution over the sample volume. As can be seen from figure 12, the surface and the bulk properties of this sample were, indeed, similar. Its $\Delta V_a(x)$ value lies significantly below the dependence plotted as a dashed line and falls onto the straight solid line with a slope of $\beta = 2.15$ Å^3 per metal atom per H(D) atom. This straight line is likely to represent the $\Delta V_a(x)$ dependence for homogeneous $Ni_{0.8}Fe_{0.2}H_x$ and $Ni_{0.8}Fe_{0.2}D_x$ solid solutions, as all the experimental $\Delta V_a(x)$ points for such solutions are close to it.

It also seems worth mentioning that, although the minimum diffusion rate and therefore the maximum inhomogeneity of the $Ni_{0.8}Fe_{0.2}H_x$ and $Ni_{0.8}Fe_{0.2}D_x$ solutions should be expected for hydrogen contents around $x = 0.5$, the maximum difference between the mean hydrogen content of thick samples and their nearly equilibrium surface content should be observed at a higher hydrogen concentration. This is because the number of hydrogen atoms that must diffuse through the sample surface to achieve the equilibrium concentration increases with increasing concentration, whereas the time of hydrogenation is fixed. The observed maximum deviation of the x-ray non-equilibrium $\Delta V_a(x)$ values (open symbols in figure 12) from the straight solid line at $x \approx 0.7$–0.8 agrees with this picture.

Thus, the $\Delta V_a(x)$ dependence for homogeneous $Ni_{0.8}Fe_{0.2}H_x$ and $Ni_{0.8}Fe_{0.2}D_x$ solid solutions is close to the straight line with a slope of $\beta = (\partial/\partial x)\Delta V_a(x) = 2.15$ Å^3 per metal atom per H(D) atom. The non-linearity of the $\Delta V_a(x)$ dependences of the $Ni_{0.8}Fe_{0.2}H_x$ solid solutions constructed earlier [39] and in the present paper was a result of two factors:

(i) the samples of intermediate concentrations were prepared in the T–P range of supercritical anomalies of the isomorphous $\gamma_1 \leftrightarrow \gamma_2$ transformation, and they remained in an inhomogeneous, non-equilibrium state due to the low H diffusion rate, and
(ii) the lattice parameters of these samples were determined by x-ray diffraction that scanned a thin surface layer where the hydrogen concentration was higher than in the bulk, and these parameters were then related to the mean hydrogen content of the samples.

Similar non-linear $\Delta V_a(x)$ dependences for hydrogen solid solutions in other fcc nickel alloys and in fcc palladium alloys [9] are likely to have the same origin, because samples of intermediate compositions in these systems also were synthesized in the T–P ranges of supercritical anomalies and studied by x-ray diffraction.

3.3.2. ^{57}Fe *Mössbauer investigation.* The local distribution of hydrogen around iron atoms can be examined by ^{57}Fe Mössbauer spectroscopy. It has been shown for a wide range of metal hydrides that the Mössbauer isomer shift S is proportional to the number of hydrogen atoms surrounding the iron probes, the proportionality constant ranging from 0.08 to 0.10 mm s^{-1} per hydrogen atom [42, 43]. In Mössbauer transmission experiments, the measured isomer shift represents an average over the bulk of the investigated sample.

The samples used for Mössbauer spectroscopy were 0.08 mm thick foils hydrogenated at 250 °C. They were measured at 4.2 K with a source of ^{57}Co in rhodium also at a temperature

Table 3. The Mössbauer isomer shifts S for $Ni_{0.8}Fe_{0.2}H_x$ samples. N_H is the estimated average number of H atoms surrounding an Fe atom; N_{Fe} is the average number of Fe atoms surrounding a H atom; $\langle N_{Fe}\rangle = 1.2$ is the average number of Fe atoms surrounding an arbitrary octahedral interstitial position.

x	S (mm s^{-1})	N_H	N_{Fe}	$N_{Fe}/\langle N_{Fe}\rangle$
0.000	−0.101	0.00	—	—
0.044	−0.098	0.03	0.15	0.13
0.152	−0.080	0.24	0.32	0.27
0.829	0.310	4.84	1.17	0.98
0.846	0.338	5.17	1.22	1.02
0.973	0.399	5.89	1.21	1.01
0.995	0.406	5.97	1.20	1.00

of 4.2 K. The isomer shifts S of the studied samples are listed in table 3. The $S(x)$-dependence obtained is significantly non-linear at low x-values. This directly corresponds to a non-linear dependence of the number of hydrogen atoms around the Fe probes.

Somewhat more quantitative information can be obtained by employing a rough model: assuming that in the nearly fully hydrogenated sample with $x = 0.995$ the remaining empty octahedral interstitials are randomly distributed over the sample, one obtains $N_H = 6\times 0.995 = 5.97$ for the average number of hydrogen atoms around an iron (six being the number of octahedral interstitial positions surrounding an fcc metal site). Comparing the isomer shift $S = 0.406$ mm s^{-1} of this sample with $S_0 = -0.101$ mm s^{-1} for a hydrogen-free $Ni_{0.8}Fe_{0.2}$ sample yields $dS = 0.085$ mm s^{-1} for the isomer shift induced by a single hydrogen neighbour. With this value it is possible to calculate the mean number of hydrogen atoms around iron for all investigated samples. The results are shown in table 3.

It is instructive to also calculate the corresponding number N_{Fe} of iron atoms around a given hydrogen atom. By counting the number of Fe–H 'bonds' one arrives at $N_{Fe} = yN_H/x$, where y is the iron content in a $Ni_{1-y}Fe_y$ alloy. N_{Fe} (table 3) should be compared with the average number $\langle N_{Fe}\rangle = 6y = 1.2$ of Fe atoms surrounding an arbitrary octahedral interstitial position in a random alloy. As one can see, N_{Fe} is significantly smaller than $\langle N_{Fe}\rangle$ in the weakly loaded $Ni_{0.8}Fe_{0.2}$ samples, where the hydrogen selects sites with no or few iron neighbours. This shows that interstitial positions near Fe atoms are energetically less favourable for hydrogen than positions without or with relatively few Fe neighbours. The observed non-uniform distribution of hydrogen atoms over the interstitial positions is a typical example of partial thermodynamic equilibrium in a system where one component, namely hydrogen, can move freely, while the other components are frozen.

4. Conclusions

The variety of results discussed in this paper were mostly obtained by studying Fe–H and Fe–Me–H samples synthesized under hydrogen pressures up to 9 GPa at temperatures up to 400 °C. We believe, however, that interesting properties and unusual effects in the Fe–H and related systems are by no means exhausted with the findings already made. It seems that the most promising means to gain new results is an increase of the synthesis temperature, which, for example, might give a chance to produce and study rather concentrated α (bcc) solutions of hydrogen in iron. Such solutions have never been synthesized for any other d metal in groups VI–VIII. In this context some results of the Japanese group from Chuo University [44–46] look very encouraging, and it is worth concluding this paper with a brief description of their findings.

One of the most prominent results of the Japanese group is the discovery of a sluggish irreversible transition occurring in some metals (Pd, Ni, Ti, Al and Mo, see [44] for references) in a hydrogen atmosphere at high temperatures. The transition lasts for hours and is accompanied by a significant decrease in the lattice parameters of the hydrides initially formed under the same pressure and temperature. The authors ascribe this transition to the formation of a very large number of vacancies in the metal lattice, up to 20 at.%. No such transition, though, was observed in the ε' and γ hydride of iron in the course of an *in situ* x-ray investigation at a hydrogen pressure of 6 GPa and temperatures to 800 °C [10]. Nevertheless, the analysis of hydrogen desorption from α-FeH_x samples exposed to a hydrogen pressure of 1.7 GPa and temperatures of 300–600 °C for 2 h revealed the presence of 0.1–1.5 at.% hydrogen, which was concluded to be trapped mostly by vacancies in the metal lattice [44].

Moreover, a new phase was observed in the Fe–H system at 6 GPa and 900–1200 °C [45]. Most lines of the powder x-ray diffraction pattern of that phase could be indexed assuming a simple-cubic structure with $a = 2.916(3)$ Å at 1000 °C, noticeably exceeding the lattice parameter of α-Fe under the same pressure and temperature in an inert medium. The authors tentatively identified the new phase as iron hydride with a defect bcc structure, in which a large number of vacancies exist in one of the two simple-cubic sublattices of bcc Fe.

The *in situ* x-ray investigation of the hydrogen-exchange reaction between FeTi–H hydride and Fe at a pressure of 3 GPa showed [46] that γ hydride of iron formed at 700 °C and rapidly cooled below 150 °C transforms to a non-equilibrium α-FeH_x solution oversaturated with hydrogen. The hydrogen content of the α-FeH_x solution was roughly estimated from the expansion of the bcc Fe lattice and reached $x \approx 0.04$–0.13 [46], significantly exceeding the equilibrium value of $x < 0.01$ [20].

The above results, of course, need further verification, but any of them, if valid, opens interesting perspectives for studies of bcc hydrides of iron and its alloys. If, for example, a quenched sample of α-$FeH_{0.13}$ is retained at ambient pressure, its hydrogen content will be large enough for a reliable determination of hydrogen positions in the bcc Fe lattice by neutron diffraction and for the investigation of the effect of hydrogen on the magnetic properties of α-Fe by Mössbauer spectroscopy and magnetization measurements, to mention only a few possibilities.

Acknowledgment

The support from the Russian Foundation for Basic Research under grant No 99-02-17299 is gratefully acknowledged.

References

[1] Larin VN 1975 *Hydrided Earth: the New Geology of our Primordially Hydrogen-Rich Planet* (Moscow: Izd. IMGRE) in Russian
Larin V N 1993 *Hydrided Earth: the New Geology of our Primordially Hydrogen-Rich Planet* (Calgary: Polar)
[2] Badding J V, Mao H K and Hemley R J 1992 *High-Pressure Research: Application to Earth and Planetary Sciences* ed Y Syono and M H Manghnani (Tokyo: Terra) pp 363–71
[3] Fukai Y 1992 *High-Pressure Research: Application to Earth and Planetary Sciences* ed Y Syono and M H Manghnani (Tokyo: Terra) pp 373–85
[4] da Silva J R G and McLellan R B 1976 *J. Less-Common Met.* **50** 1–5
[5] Schreyer F, Frech G, Wolf G K and Wagner F E 1983 *Solid State Commun.* **46** 647–50
[6] Antonov V E, Belash I T, Degtyareva V F, Ponyatovskii E G and Shiryaev V I 1980 *Dokl. Akad. Nauk SSSR* **252** 1384–7 (Engl. transl. 1980 *Sov. Phys.–Dokl.* **25** 490)
[7] Ponyatovsky E G, Antonov V E and Belash I T 1984 *Problems in Solid-State Physics* ed A M Prokhorov and A S Prokhorov (Moscow: Mir) pp 109–72

[8] Antonov V E, Antonova T E, Chirin N A, Ponyatovsky E G, Baier M and Wagner F E 1996 *Scr. Mater.* **34** 1331–6
[9] Fukai Y 1992 *The Metal–Hydrogen System* (Berlin: Springer) p 97
[10] Yamakata M, Yagi T, Utsumi W and Fukai Y 1992 *Proc. Japan. Acad.* B **68** 172–6
[11] Badding J V, Hemley R J and Mao H K 1991 *Science* **253** 421–4
[12] Choe I, Ingalls R, Brown J M, Sato-Sorensen Y and Mills R 1991 *Phys. Rev.* B **44** 1–4
[13] Tkacz M 2002 *J. Alloys Compounds* **330–332** 25–8
[14] Somenkov V A and Shil'stein S Sh 1979 *Z. Phys. Chem., NF* **117** 125–44
[15] Fedotov V K, Antonov V E, Antonova T E, Bokhenkov E L, Dorner B, Grosse G and Wagner F E 1999 *J. Alloys Compounds* **291** 1–7
[16] Antonov V E, Belash I T, Degtyareva V F, Mogilyansky D N, Ponomarev B K and Shekhtman V Sh 1989 *Int. J. Hydrogen Energy* **14** 371–7
[17] Schneider G, Baier M, Wordel R, Wagner F E, Antonov V E, Ponyatovsky E G, Kopilovskii Yu and Makarov E 1991 *J. Less-Common Met.* **172–174** 333–42
[18] Antonov V E, Cornell K, Fedotov V K, Kolesnikov A I, Ponyatovsky E G, Shiryaev V I and Wipf H 1998 *J. Alloys Compounds* **264** 214–22
[19] Antonov V E, Belash I T, Ponyatovskii E G, Thiessen V G and Shiryaev V I 1981 *Phys. Status Solidi* a **65** K43–8
[20] Antonov V E, Belash I T and Ponyatovsky E G 1982 *Scr. Metall.* **16** 203–8
[21] Baranowski B 1972 *Ber. Bunsenges. Phys. Chem.* **76** 714–24
[22] Tonkov E Yu 1992 *High Pressure Phase Transformations. A Handbook* vol 2 (Philadelphia, PA: Gordon and Breach) pp 388–91
[23] Wordel R, Wagner F E, Antonov V E, Ponyatovskii E G, Permogorov A, Plachinda A and Makarov E F 1985 *Z. Phys. Chem., NF* **146** 121–7
Wordel R, Wagner F E, Antonov V E, Ponyatovskii E G, Permogorov A, Plachinda A and Makarov E F 1986 *Hyperfine Interact.* **28** 1005–8
[24] Glazkov V P, Irodova A V, Somenkov V A, Shil'shtein S Sh, Antonov V E and Ponyatovskii E G 1984 *Fiz. Tverd. Tela* **26** 3261–5 (Engl. transl. 1984 *Sov. Phys.–Solid State* **26** 1961–63)
[25] Cornell K, Wipf H, Antonov V E, Antonova T E, Kolesnikov A I, Ponyatovsky E G and Dorner B 1997 *Pol. J. Chem.* **71** 1792–6
[26] Rowe J M, Rush J J, Smith H G, Mostoller M and Flotow H E 1974 *Phys. Rev. Lett.* **33** 1297–300
[27] Ross D K, Martin P F, Oates W A and Khoda Bakhsh R 1979 *Z. Phys. Chem., NF* **114** 221–30
[28] Antonov V E, Cornell K, Dorner B, Fedotov V K, Grosse G, Kolesnikov A I, Wagner F E and Wipf H 2000 *Solid State Commun.* **113** 569–72
[29] Ponyatovskii E G, Antonov V E and Belash I T 1982 *Usp. Fiz. Nauk* **137** 663–705 (Engl. transl. 1982 *Sov. Phys.–Usp.* **25** 596–619)
[30] Belash I T, Malyshev V Yu, Ponomarev B K, Ponyatovsky E G and Sokolov A Yu 1986 *Fiz. Tverd. Tela* **28** 1317–23 (Engl. transl. 1986 *Sov. Phys.–Solid State* **28** 741–4)
[31] Ohno H 1971 *J. Phys. Soc. Japan* **31** 92–101
[32] Ohno H and Mekata M 1971 *J. Phys. Soc. Japan* **31** 102–8
[33] Antonov V E, Belash I T, Georgieva I Ya, Degtyareva V F, Thiessen V G and Shalimova A V 1982 *Fiz. Tverd. Tela* **24** 975–81 (Engl. transl. 1982 *Sov. Phys.–Solid State* **24** 554–8)
[34] Irodova A V, Glazkov V P, Somenkov V A, Shil'shtein S Sh, Antonov V E and Ponyatovskii E G 1987 *Fiz. Tverd. Tela* **29** 2714–20 (Engl. transl. 1987 *Sov. Phys.–Solid State* **29** 1562–5)
[35] Khan H R and Raub Ch J 1976 *J. Less-Common Met.* **43** 399–406
[36] Dubiel S M and Inden G 1987 *Z. Metallk.* **78** 544–9
[37] Antonov V E, Belash I T and Ponyatovskii E G 1977 *Dokl. Akad. Nauk SSSR* **233** 1114–7 (in Russian)
[38] Ponyatovskii E G, Antonov V E and Belash I T 1976 *Dokl. Akad. Nauk SSSR* **230** 649–51 (in Russian)
[39] Antonov V E, Belash I T, Degtyareva V F, Ponomarev B K, Ponyatovskii E G and Tissen V G 1978 *Fiz. Tverd. Tela* **20** 2680–6 (Engl. transl. 1978 *Sov. Phys.–Solid State* **20** 1548–52)
[40] Tsuschida T 1963 *J. Phys. Soc. Japan* **18** 1016–9
[41] Baranowski B, Skośkiewicz T and Szafrański A W 1975 *Fiz. Nizk. Temp.* **1** 616–23
[42] Pröbst F and Wagner F E 1987 *J. Phys. F: Met. Phys.* **17** 2459–74
[43] Baier M 1994 Mössbauerspektroskopische Untersuchungen an Metall-Wasserstoff-Systemen *PhD Thesis* Technische Universität München
[44] Iwamoto M and Fukai Y 1999 *Mater. Trans. JIM* **40** 606–11
[45] Fukay Y and Yamakata M 1993 *Z. Phys. Chem., NF* **179** 119–23
[46] Fukai Y, Fukizawa A, Watanabe K and Amano M 1982 *Japan. J. Appl. Phys.* **21** L318–20